International Journal of Nanomedicine

Dovepress
open access to scientific and medical research

Open Access Full Text Article

ORIGINAL RESEARCH

Co-loading antioxidant N-acetylcysteine attenuates cytotoxicity of iron oxide nanoparticles in hypoxia/reoxygenation cardiomyocytes

This article was published in the following Dove Press journal:
International Journal of Nanomedicine

Yunli Shen[1,*]
Shiyu Gong[1,*]
Jiming Li[1,*]
Yunkai Wang[1]
Xumin Zhang[1]
Hao Zheng[1]
Qi Zhang[1]
Jieyun You[1]
Zheyong Huang[2]
Yihan Chen[1]

[1]Department of Cardiology, Shanghai East Hospital, Tongji University School of Medicine, Shanghai 200120, People's Republic of China; [2]Shanghai Institute of Cardiovascular Diseases, Zhongshan Hospital, Fudan University, Shanghai 200032, People's Republic of China

*These authors contributed equally to this work

Purpose: Myocardial delivery of magnetic iron oxide nanoparticles (MNPs) might produce iron overload-induced myocardial injury, and the oxidative stress was regarded as the main mechanism. Therefore, we speculated antioxidant modification might be a reasonable strategy to mitigate the toxicity of MNPs.

Methods and results: Antioxidant N-acetylcysteine (NAC) was loaded into magnetic mesoporous silica coated Fe_3O_4 nanoparticles. Neonatal rat hypoxia/reoxygenation (H/R) cardiomyocytes were incubated with nanoparticles for 24 hrs. NAC can effectively mitigate iron-induced oxidative injury of cardiomyocytes, evidenced by reduced production of MDA, 8-iso-PGF2α, and 8-OHDG and maintained concentrations of SOD, CAT, GSH-Px, and GSH in ELISA and biochemical tests; downregulated expression of CHOP, GRP78, p62, and LC3-II proteins in Western Blot, and less cardiomyocytes apoptosis in flow cytometric analysis.

Conclusions: NAC modifying could suppress the toxic effects of Fe_3O_4 nanoparticles in H/R cardiomyocytes model in vitro, indicating a promising strategy to improve the safety of iron oxide nanoparticles.

Keywords: N-acetylcysteine (NAC), iron oxide nanoparticles, oxidative stress, cardiomyocytes, hypoxia-reoxygenation

Introduction

Owing to their superparamagnetic and magnetic responsive properties, magnetic iron oxide nanoparticles (MNPs) have been widely used as magnetic resonance contrast agents or magnetic targeting carriers in the imaging, diagnosis, cells, and drug/gene delivery for cardiovascular diseases.

Although MNPs do not significantly reduce viability and proliferation potential of stem cells,[1] it is usually believed that its cytotoxic effects were related to the dose and duration of iron exposure.[2,3] The most extreme example is iron overload cardiomyopathy, in which myocardial iron overload at a long time and high dose ultimately led to severe even lethal diastolic and systolic heart failure.[4,5] Actually, the cytotoxic risk also existed even in the diagnostic or therapeutic administration of MNPs. The toxicity of MNPs in promoting coagulation and inducing cardiac oxidative stress has been confirmed in mice 24 hrs following intravenous injection.[6] Intraperitoneal injection of Fe_2O_3 nanoparticles twice a week at doses of 25 and 50 mg/kg at intervals of 7 days within 30 days led to oxidative cardiomyocytes degeneration and cardiac dysfunction through apoptosis and necrosis in mice.[7] Recently, we found that iron could be

Correspondence: Zheyong Huang
Shanghai Institute of Cardiovascular Disease, Zhongshan Hospital, Fudan University, 180 Feng Lin Road, Shanghai 200032, People's Republic of China
Tel +86 0 216 404 1990
Email zheyonghuang@126.com

Yihan Chen
Department of Cardiology, Shanghai East Hospital, Tongji University School of Medicine, 150 Ji Mo Road, Shanghai 200120, People's Republic of China
Tel +86 0 213 880 4518
Email yihanchen@tongji.edu.cn

submit your manuscript | www.dovepress.com
DovePress
http://doi.org/10.2147/IJN.S209820

accumulated in the infarcted myocardium as long as at least 6 months when locally intramyocardial injection of MNPs labeled stem cells in rats.[8] Therefore, it is reasonable to presume that local myocardial administration of MNPs-mediated diagnostic or therapeutic agents might cause myocardial iron overload, consequently aggravating negative remodeling of ischemic myocardium and deterioration of cardiac function.

The oxidative stress was widely regarded as the main mechanism of MNPs induced injury.[7,9–14] Thus, antioxidant modification might be a promising strategy to mitigate the toxicity of MNPs. We hypothesize that MNPs modified with antioxidant could significantly reduce the toxicity of ischemic cardiomyocytes caused by iron oxide nanoparticles. Here, we loaded N-acetylcysteine (NAC), a potent antioxidant,[15–17] into magnetic mesoporous silica nanoparticles (M-MSN), thus to construct M-MSN@NAC. We further tested whether M-MSN@NAC could suppress the toxic effects of MNPs or M-MSNs in a hypoxia/reoxygenation (H/R) cardiomyocytes model.

Materials and methods

Preparation of M-MSNs and M-MSN@NAC

Cetyltrimethylammonium bromide (CTAB), tetraethyl orthosilicate (TEOS), and ammonium nitrate (NH_4NO_3) were obtained from Fluka. Ethyl acetate, ethanol, cyclohexane, and methanol were purchased from Sinopharm Chemical Reagent Co., Ltd., China. All these reagents are analytical reagent grade and used as received without any further purification. All of the other chemicals were obtained from Sigma (St. Louis, MO, USA) except where noted. Millipore water (18.2 MΩ.cm^{-1}) was used in the preparations of all aqueous solutions.

The schematic diagram of the synthesis of M-MSN@NAC was shown in Figure 1A. M-MSNs were synthesized according to the reference as follows:[18] The magnetic Fe_3O_4 nanoparticles (MNPs) dispersed in chloroform were synthesized by the co-precipitation method with oleic acid surface.[19] First, 0.74 mL MNPs solutions (6.0 mg Fe/mL) was added into 5 mL CTAB aqueous solution (0.08 M). After 30 mins of

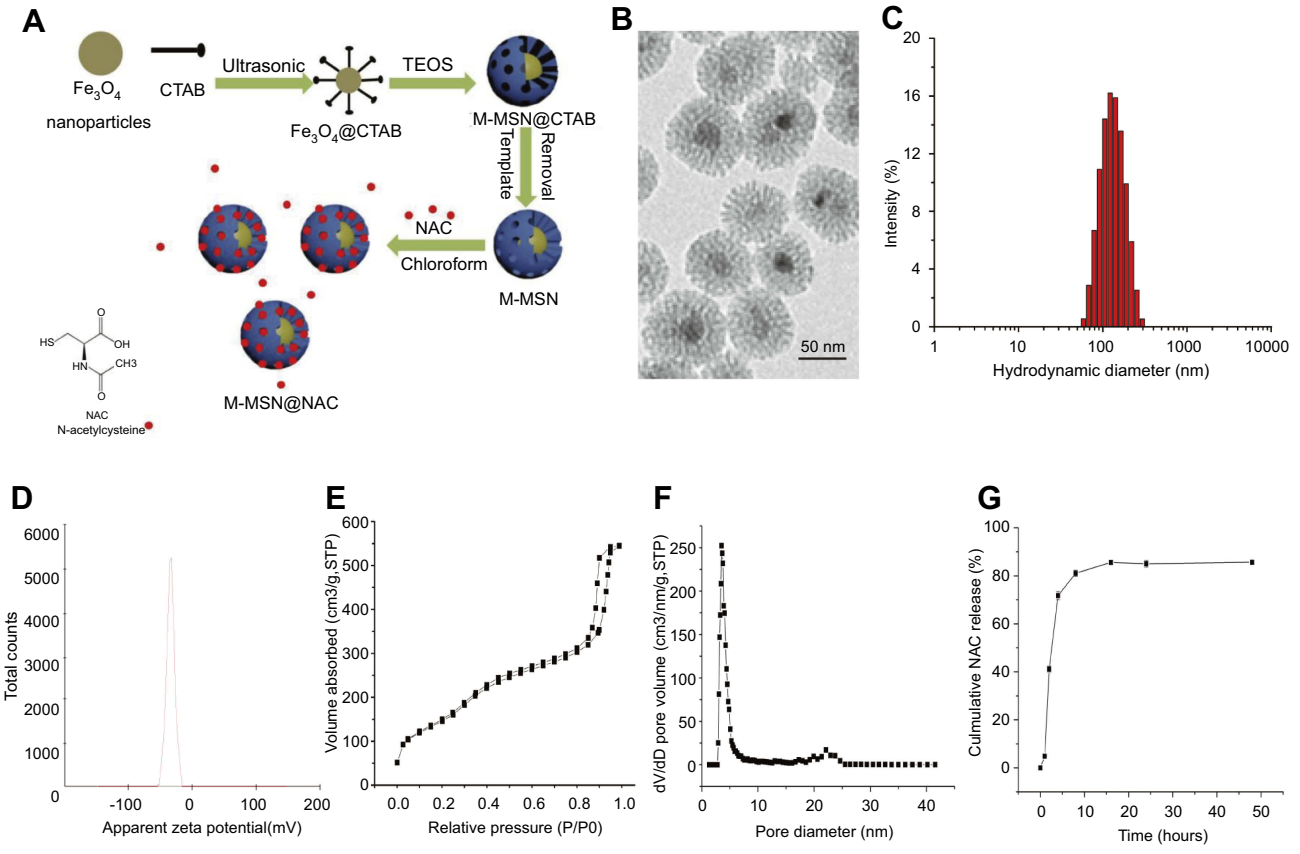

Figure 1 Characterization of the M-MSN@NAC. (**A**) Schematic diagram of synthesis of M-MSN@NAC. (**B**) Representative TEM image. (**C**) Hydrodynamic diameter distribution of M-MSN@NAC in PBS. (**D**) Zeta potential distribution of M-MSN@NAC. (**E**) Nitrogen sorption isotherm at 77 K. (**F**) The corresponding pore size distribution. (**G**) Profile of NAC release from the M-MSN@NAC dissolved in PBS (pH=7.4) at 37°C. Data were collected from three independent experiments.

Abbreviations: CTAB, cetyltrimethylammonium bromide; TEOS, tetraethyl orthosilicate; M-MSN, magnetic mesoporous silica nanoparticles; NAC, N-acetylcysteine; M-MSN@NAC, M-MSN loaded with NAC; TEM, transmission electron microscopy.

continuous ultrasonication at 50°C, the mixture was stirred at 70°C for another 10 mins to evaporate the solvent for obtaining a transparent black solution. Second, 45 mL water, 0.5 mL TEOS, 3 mL ethyl acetate, and 0.3 mL NaOH solution (2 M) were added to the obtained dispersion, and then the mixture was stirred at 70°C with refluxing for 3 hrs. Finally, the nanoparticles were collected by centrifugation and washed with ethanol/water three times, while the CTAB template was removed by a highly efficient ion-exchange method.

To load NAC into M-MSNs, 20 mg M-MSNs were suspended into 20 mL chloroform solution of NAC (20 mg/mL). The mixture was incubated at 25°C for 2 hrs after ultrasonication for 5 mins, and the non-loaded NAC was removed from solution by centrifugation. The residual NAC-loaded M-MSNs (M-MSN@NAC) were collected, and the solution was measured by UV-Vis method at a wavelength of 562 nm to calculate the concentrations of NAC.[20]

Characterization of M-MSN@NAC

Nitrogen adsorption measurement was done at 77 K using Quadrasorb SI analyzer (Quantachrome Corporation, USA). The specific surface areas were calculated by the BET method using adsorption data. The pore size distribution was determined by analyzing the adsorption branch by the BJH method. Morphology of M-MSNs was analyzed using a JEM 2010 (JEOL, Japan) transmission electron microscopy (TEM) instrument with 200 kV accelerated voltage. Dynamic light scattering (DLS) measurements were performed on a Zeta sizer Nano instrument (Malvern, UK) at 298 K to analyze the hydrodynamic diameters and Zeta potential of M-MSN@NAC. The concentrations of NAC were detected on a NanoDrop 1000 spectrophotometer (Thermo Scientific, USA).

Assays of NAC release from M-MSN@NAC

To determine the drug release profile from the M-MSN@NAC, 10 mg M-MSN@NAC were dispersed in 2 mL of phosphate-buffered saline (PBS, pH=7.4), and the dispersion was transferred into a dialysis bag with a molecular weight cut off of 1000 Da. The dialysis was then kept in 18 mL PBS at 37°C and shaken at a speed of 150 rpm. At different time intervals, 0.2 mL of the solution was collected to detect the amount of released NAC by UV-Vis. To keep constant volume, 0.2 mL of fresh PBS was added after each sampling. All NAC release results were averaged with three measurements.

Primary culture of neonatal rat cardiomyocytes and hypoxia/reoxygenation (H/R) procedure

The rats aged from 1 to 3 days were purchased from Shanghai animal administration center, and then primary rat cardiomyocytes were isolated and cultured as described previously.[21] Cardiomyocytes were cultured for at least 3 days before H/R procedure. The cells were placed in a hypoxia incubator chamber (STEMCELL Technologies, Vancouver, BC, Canada) with an anoxic mixture gas (95% N_2 and 5% CO_2) for 3 hrs at 37°C followed by reoxygenation for 3 hrs with fresh culture medium (95% air and 5% CO_2) to simulate ischemic/reperfusion injury of cardiomyocytes when growing to 70–80% confluence. Animal experiments were approved by the Animal Care and Use Committee of Tongji University in compliance with the "Guide for the Care and Use of Laboratory Animals" published by the National Academy Press (NIH Publication No. 85-23, revised 1996).

Different nanoparticles (NPs) treatment

H/R cardiomyocytes were washed in PBS and then randomly divided into five groups. Except for the H/R group, which was not treated with any nanoparticles, the other four groups of H/R cardiomyocytes were incubated with 1 mL of MNPs (Fe_3O_4 50 μg/mL), M-MSNs (Fe_3O_4 50 μg/mL and MSNs 668.34 μg/mL), MSNs (MSNs 668.34 μg/mL), or M-MSN@NAC (Fe_3O_4 50 μg/mL, MSNs 668.34 μg/mL and NAC 115 μg/mL) for 24 hrs following H/R procedure, respectively. Cardiomyocytes in the control group were not subjected to hypoxia-reoxygenation procedures and incubated in serum-free DMEM for equivalent durations.

Determination of cytotoxicity

To visualize the internalization of iron oxide nanoparticles, Prussian blue staining (potassium ferrocyanide and HCl solution from Jueshen Bio-Technology Co. Ltd., Shanghai, China) and a JEM 2010 (JEOL, Japan) TEM were employed to indicate the presence and accumulation of intracellular iron particles. Cytotoxicity was assessed by detection of cell viability and lactate dehydrogenase (LDH) activity in the medium using CCK-8 and LDH assay kits (Nanjing Jiancheng Bioengineering Institute, China), respectively. For CCK-8 assay, cells in 96-well plates were treated according to the experimental procedure and then incubated with 10% CCK-8 reagents and 90% fresh DMEM media for 60 mins at 37°C before the

assay was performed. Media in 6-well plates were centrifugalized to gather supernatant for LDH activity test. All operations complied with the manufacturer's instructions.

Detection of mitochondrial membrane potential (MMP)

MMP was determined using the Mitochondrial Permeability JC-1 dye (Molecular probe). After H/R cardiomyocytes were incubated with or without different NPs for 24 hrs, cells were rinsed with PBS twice, stained with 1 mL culture medium containing 5 mmol/L JC-1 and Hoechst 33342 (10 μg/ml; Keygen Biotech, Nanjing, China) for 30 mins at 37°C. Next, cells were resuspended in 200 mL ice-cooled PBS, and fluorescence images were instantly obtained using green or red channels and the intensity ratio of the red/green fluorescence of each cardiomyocyte was measured using ImageJ (version 1.45).

Assessment of cell apoptosis

Cell apoptosis was tested using the Annexin V-Propidium Iodide (PI) apoptosis detection kit (BD Biosciences, San Diego, USA). Briefly, the collected cells were incubated with 2 mL Annexin V-FITC and 2 mL PI successively after exposed to different NPs for 24 hrs according to the manufacturer's instructions. Next, the cells were analyzed by flow cytometry within 1 hr. The identification of early and late apoptotic cells, viable or necrotic cells was referred to previous research methods.[15] The data were analyzed using BD FACS Diva software (Becton Dickinson, USA). Each treatment was performed in triplicate.

Measurement of ROS production and oxidant/antioxidant capacity

The dihydroethidium (DHE) staining was employed to detect ROS production after cardiomyocytes exposed to different nanoparticles for 24 hrs. The molecular probes DHE are nonfluorescent when not oxidized by intracellular ROS. DHE oxidized in the presence of a superoxide radical to fluorescent 2-hydroethidium (EOH), which is stable within the cell, allowing for precise measurement of DHE fluorescence without risk of interconversion variability.[22]

The levels of measurement of malonaldehyde (MDA), 8-iso-prostaglandin F2α (8-iso-PGF2α) and 8-hydroxydeoxyguanine (8-OHDG) 24 hrs after treatment were determined by an enzyme-linked immunosorbent assay (ELISA) technique with commercially available kit (Cayman Chemicals, Michigan, USA).

All samples preparation was conducted in an acrylic glovebox station for anaerobic work (MBRAUN, MB GB 2202, Germany) with the use of nitrogen (Linde Gaz, Poland) in order to prevent oxidation of sample components. The activities of superoxide dismutase (SOD), glutathione peroxidase (GSH-Px), catalase (CAT), and glutathione (GSH) in H/R cardiomyocytes from different treatment groups 24 hrs after treatment were determined with the use of commercial diagnostic kits (Shanghai Fengxiang Biotechnology Co., Ltd., China).

Detection of the related proteins of apoptosis, endoplasmic reticulum (ER) stress, and autophagy by Western blotting (WB)

Twenty-four hours after exposure, WB was performed by referring to the method of Towbin et al, 1979 with some modifications.[23] Proteins (50e100 mg) were incubated with different antibodies, ie, CCAAT/enhancer binding protein-homologous protein (CHOP), glucose-regulated protein 78 (GRP78), p62, microtubule-associated protein light chain 3 (LC3)-I/II, pro-caspase-3, cleaved caspase-3, Bax and Bcl-2 (Cell Signalling Technologies Boston, MA) after resolved on 10–12% SDS-PAGE and then electroblotted onto nitrocellulose membranes. Immunoblots were tested using horseradish peroxidase conjugated anti-mouse or anti-rabbit IgG using chemiluminescence kit and visualized by Versa Doc Imaging System (Biorad, CA, USA). Densitometric measurements of the bands were performed with digitalized scientific software program, UN-SCAN-IT, which was purchased from Silk Scientific Corporation (Orem, UT, USA). Data were expressed as the relative density of protein bands normalized to GAPDH.

Statistical analysis

All experiments were performed in triplicate at a minimum. The data were expressed as the means±standard deviation (SD) and analyzed by one-way analysis of variance (ANOVA) and the least-significant difference (LSD) test. Statistical significance was set at $p<0.05$. The statistical analysis was performed with SPSS version 20.0 (SPSS, Chicago, IL, USA).

Results

Characterization of the M-MSN@NAC

M-MSN@NAC possessed a typical core-shell composite structure, in which the mesoporous silica shells coated on the surface of a single Fe_3O_4 nanocrystal with an average size of less than 10 nm embedded in the center, presenting wormhole-like structure (Figure 1A and B). The representative TEM image revealed that M-MSN@NAC have a uniform and discrete spherical shape with a diameter of 46.43±10.68 nm (Figure 1B). The hydrodynamic diameter distribution of M-MSN@NAC in PBS has a single peak centered at 101.6 nm (Figure 1C). The hydrodynamic sizes of the synthesized M-MSN@NAC are usually larger than those detected by TEM due to the existence of a hydration layer on the outside of the M-NSN@NAC in PBS and to the shrinkage of the drying M-MSN@NAC during the TEM detection, in which the hydration layer was formed by hydroxyl groups on the surface of MSN and water. The surface charge of M-MSN@NAC synthesized in this experiment, also known as zeta potential, exhibited a value of −34.63±−1.19 mV (Figure 1D), which is an essential factor in determining the stability of this particle. Even though M-MSN@NAC were suspended in PBS for 7 days, no significant aggregation was observed, indicating that M-MSN@NAC are less likely to cause microembolism owing to developing electrostatic repulsive force between M-MSN@NAC when used as magnetic targeting drug carriers or contrast agents in vivo. According to the International Union of Pure and Applied Chemistry (IUPAC) nomenclature, the nitrogen isotherm measurement for M-MSN@NAC demonstrated a type IV isotherm with the H1 hysteresis loop (Figure 1E). A secondary condensation step occurred at high relative pressure regions (P/P>0.9), which was attributed to the interparticle spaces formed by the accumulation of M-MSN@NAC. A narrow pore size distribution curve (Figure 1F) with a sharp peak centered at 3.537 nm supports the observed pore structure in Figure 1B. The great potential in loading sufficient amount of NAC was proved by the surface area and pore volume of M-MSN, which were detected to be 436.779 m^2/g and 0.816 cm^3/g, respectively. After the M-MSN@NAC dissolved in PBS (pH=7.4) at 37°C, the time course of NAC release from the M-MSN@NAC showed that NAC was rapidly released 72% within 2.5 hrs, and then NAC release slowly entered plateau phase and lasted until 48 hrs (Figure 1G).

M-MSN@NAC prevent cell damage by MNPs or M-MSNs

After 24 hrs of incubation with M-MSN@NAC, Prussian blue staining showed the internalization of iron oxide nanoparticles (Figure 2A). TEM image confirmed again the accumulation of iron-containing nanoparticles in cardiomyocytes (Figure 2B). We first observed cytotoxicity by detecting cell viability and LDH release in H/R cardiomyocytes exposed to different NPs. Cell viability in the four treatment groups and H/R group was significantly lower than that of the control group (all p<0.001) (Figure 2C). Cell viability was indistinguishable among the four treated groups and the H/R group (all p>0.05) (Figure 2C). Compared to H/R cardiomyocytes, cells exposed to MNPs and M-MSNs exhibited increased LDH release (both p<0.0001), whereas LDH activities did not show significant difference between the M-MSN@NAC group and the H/R group (Figure 2D), indicating that M-MSN@NAC can prevent cell damage mediated by MNPs or M-MSNs. Not surprisingly, LDH activities of the four treatment groups and H/R group were significantly higher than those of the control group (all p<0.001) (Figure 2D).

M-MSN@NAC reverse MMP loss and cell apoptosis induced by MNPs or M-MSNs

Compared with the control group, the four treatment groups and H/R group showed significant loss of MMP (all p<0.001) (Figure 3A and B). Compared to the H/R group, remarkable loss of MMP in cardiomyocytes was observed both in the MNP and M-MSN groups (both p<0.05) (Figure 3A and B). However, the M-MSN@NAC group demonstrated similar MMP relative to the H/R group (p>0.05) (Figure3A and 3B).

Compared with the M-MSN@NAC group, WB detection showed that both the MNP and M-MSN groups had an increased pro-apoptotic protein expression of Caspase-3 and Bax, and a reduced anti-apoptotic protein expression of Bcl-2 after exposure (all p<0.05) (Figure 4A–D). Similarly, no significant difference was found in apoptosis-related proteins between the M-MSN@NAC and H/R groups (p>0.05) (Figure 4A–D). The four treatment groups and H/R group exhibited higher expression of pro-apoptotic protein and lower expression of anti-apoptotic protein than those of the control group (all p<0.001) (Figure 4A–D).

Flow cytometry analysis showed that cell apoptosis had no significant difference among the MNP, MSN, M-

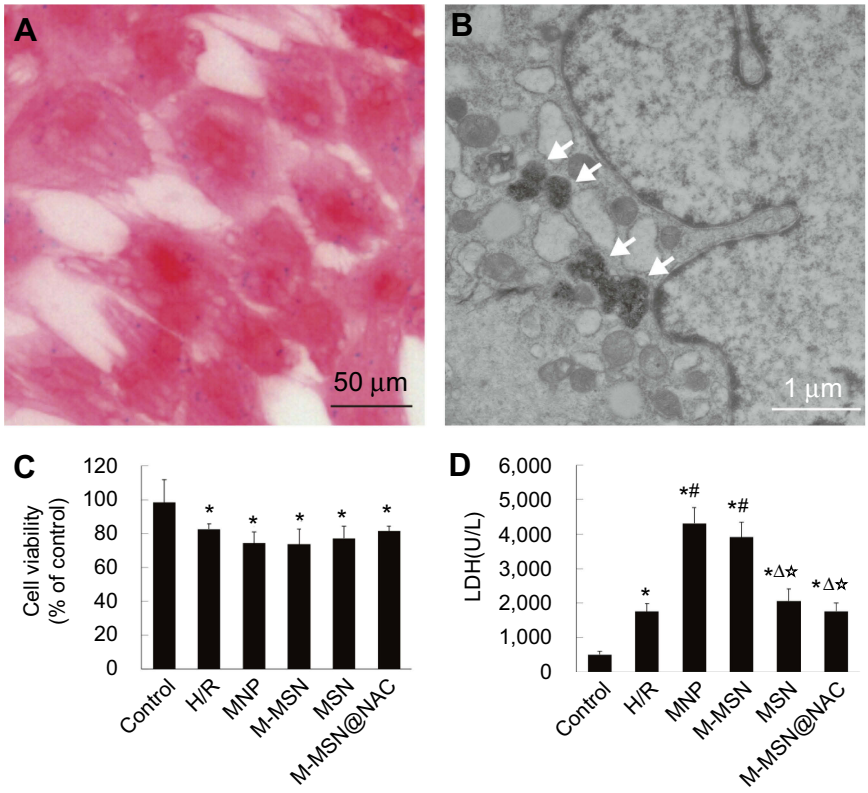

Figure 2 Effects of different NPs on cardiomyocytes viability and injury. (**A-B**) Prussian blue staining and TEM image showed the accumulation of iron-containing nanoparticles in cardiomyocytes following incubation with M-MSN@NAC for 24 hrs. White arrows denote the M-MSN@NAC or particulate matter. (**C**) Cell viability was measured by CCK-8. (**D**) Cell toxicity was evaluated by LDH leakage. Data were collected from three independent experiments. (*p<0.001 vs Control; #p<0.0001 vs H/R; Δp<0.001 vs MNP; ☆p<0.001 vs M-MSN).

Abbreviations: NPs, nanoparticles; TEM, transmission electron microscopy; LDH, lactate dehydrogenase; H/R, hypoxia/reoxygenation; MNP, magnetic iron oxide nanoparticles; MSN, mesoporous silica nanoparticles; M-MSN, magnetic mesoporous silica nanoparticles; M-MSN@NAC, M-MSN loaded with NAC.

MSN, M-MSN@NAC, and H/R groups (all p>0.05) (Figure 5A–D). Compared with the MNP and the M-MSN groups, although M-MSN@NAC group failed to show significant statistical difference, it still exhibited a tendency to reduce dead, late apoptosis, and early apoptosis cells. Cell apoptosis in the control group was significantly lower than those of the four treatment groups and H/R groups (all p<0.0001) (Figure 5A–D).

Our findings suggested that MNPs and M-MSNs might have a potential risk to exacerbate apoptosis of H/R cardiomyocytes through upregulating Caspase-3 and Bax, and downregulating Bcl-2. M-MSN@NAC could reverse the harmful effects induced by MNPs or M-MSNs (Figure 4A–D). Taken together, these data suggest that M-MSN@NAC might bear a potential to reverse cell apoptosis induced by iron oxide NPs.

M-MSN@NAC correct the imbalance of oxidation and anti-oxidation via reducing ROS generation induced by MNPs or M-MSNs

To detect oxidative stress of H/R cardiomyocytes, ROS generation was detected by DHE staining after exposure. DHE fluorescence imaging revealed that the levels of ROS in the MNP group and the M-MSN group were 1.95 times and 2.01 times greater than those in the H/R group (both p<0.001) (Figure 6A and B), respectively. Interestingly, ROS level was comparable between the M-MSN@NAC and the H/R groups (p>0.05) (Figure 6A and B), indicating that MNPs and M-MSNs intensely induce oxidative stress of H/R cardiomyocytes, but this adverse effect can be suppressed by NAC released from M-MSN@NAC.

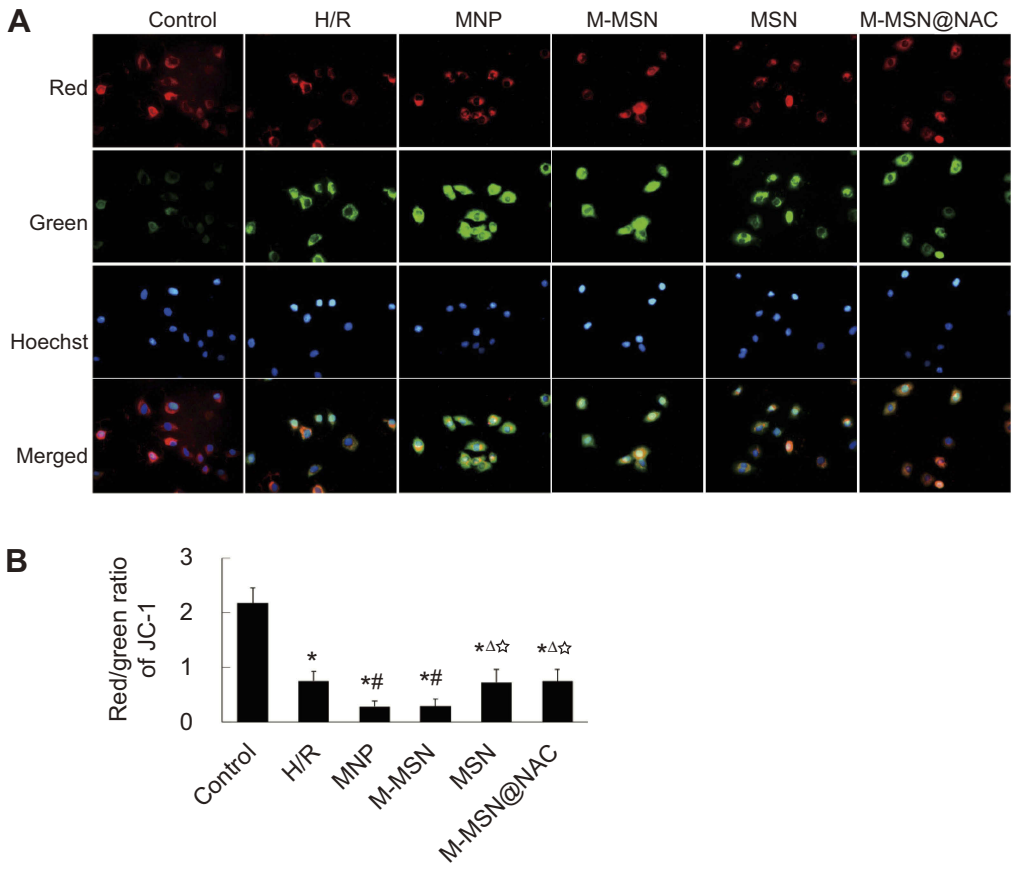

Figure 3 Effects of different NPs on cardiomyocytes MMP. (**A**) MMP was assessed by fluorescence microscopy with JC-1 staining. (**B**) Quantitative analysis of MMP by plate reader. Data were collected from three independent experiments. (*p<0.001 vs Control; #p<0.05 vs H/R; Δp<0.05 vs MNP; ☆p<0.05 vs M-MSN).

Abbreviations: NPs, nanoparticles; MMP, mitochondrial membrane potential; H/R, hypoxia/reoxygenation; MNP, magnetic iron oxide nanoparticles; MSN, mesoporous silica nanoparticles; M-MSN, magnetic mesoporous silica nanoparticles; M-MSN@NAC, M-MSN loaded with NAC.

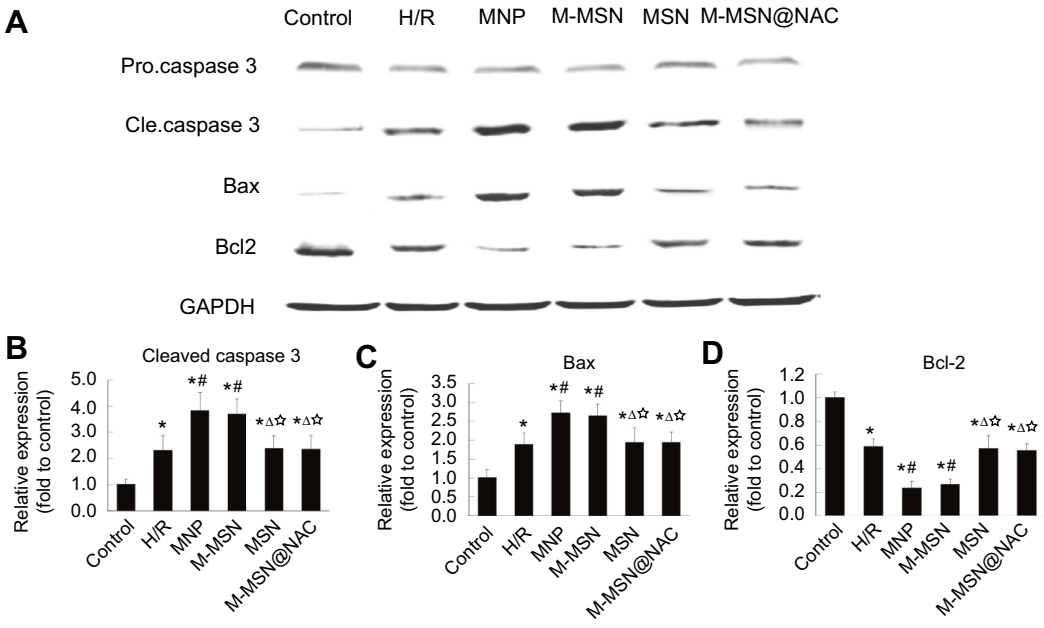

Figure 4 Expression of apoptosis-related proteins induced by different NPs. (**A**) Apoptosis-related proteins determined by WB in cardiomyocytes exposed to different NPs. (**B-D**) Quantitative analysis of cleaved caspase 3, Bax, and Bcl-2 using data from three independent experiments. (*p<0.001 vs Control; #p<0.05 vs H/R; Δp<0.05 vs MNP; ☆p<0.05 vs M-MSN).

Abbreviations: NPs, nanoparticles; WB,Western blotting; H/R, hypoxia/reoxygenation; MNP, magnetic iron oxide nanoparticles; MSN, mesoporous silica nanoparticles; M-MSN, magnetic mesoporous silica nanoparticles; M-MSN@NAC, M-MSN loaded with NAC.

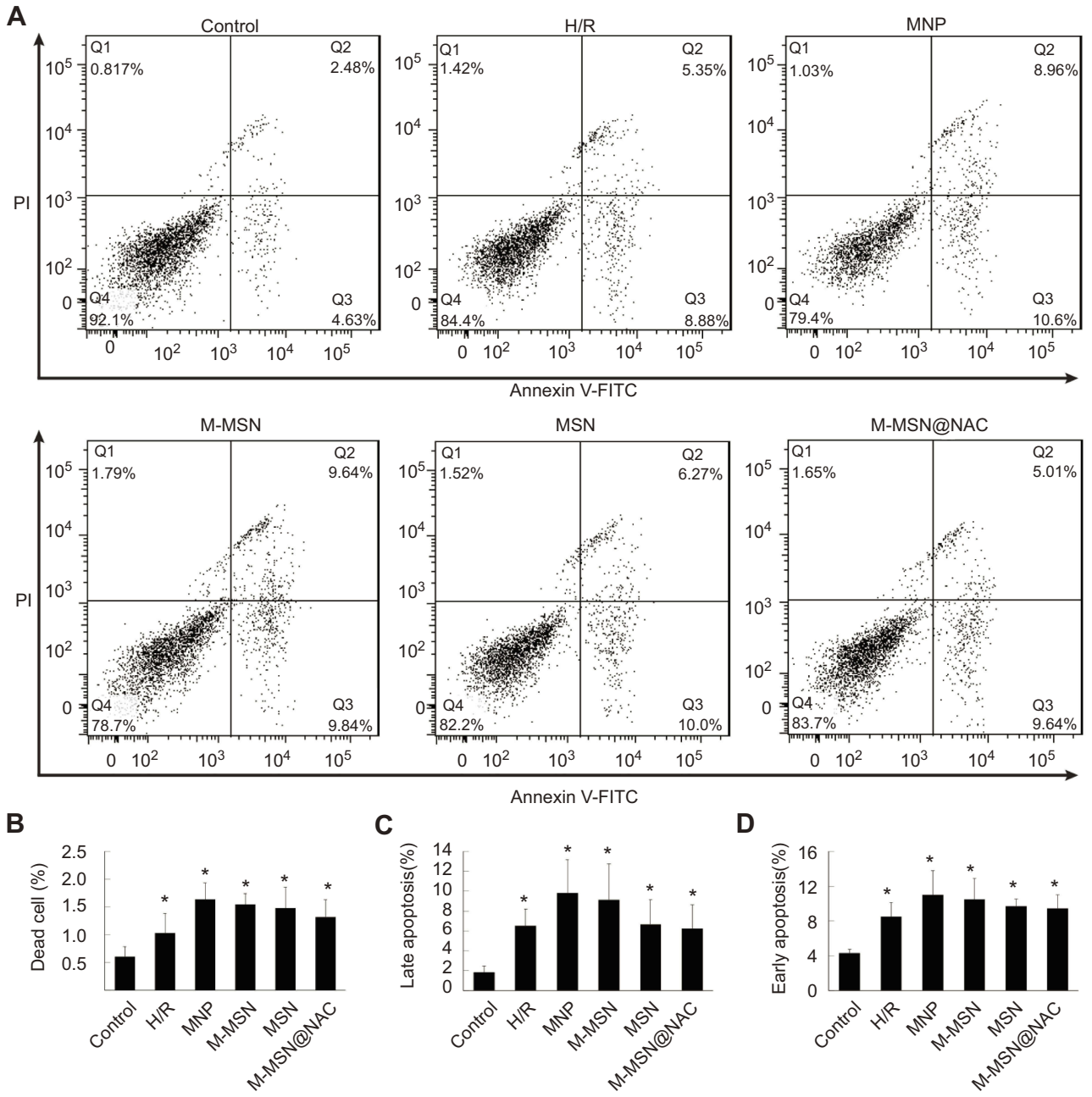

Figure 5 Cardiomyocytes death induced by exposure to different NPs. (**A**) Flow cytometric analysis of cardiomyocytes exposed to different NPs for 24 hrs. (**B-D**) Quantitative analysis of apoptotic cells by FACS analysis with Annexin V/PI staining. Data were collected from three independent experiments. There was no significant difference in cell apoptosis among the MNP, MSN, M-MSN, M-MSN@NAC, and H/R groups (all $p>0.05$) (*$p<0.0001$ vs Control).

Abbreviations: NPs, nanoparticles; H/R, hypoxia/reoxygenation; MNP, magnetic iron oxide nanoparticles; MSN, mesoporous silica nanoparticles; M-MSN, magnetic mesoporous silica nanoparticles; M-MSN@NAC, M-MSN loaded with NAC.

To further evaluate oxidative stress injury in H/R cardiomyocytes, MDA, 8-OHDG, and 8-iso-PGF2α were examined by ELISA and the action of GSH and CAT, GSH-Px, and SOD were assessed with biochemical methods, respectively. ELISA analysis at 24 hrs after exposure showed that the concentrations of MDA, 8-OHDG, and 8-iso-PGF2α in both the M-MSN group and the MNP group were significantly higher than those in the H/R group (all $p<0.01$) (Figure 6C–E), but there was no statistical significance between the M-MSN group and the MNP group ($p>0.05$) (Figure 6C–E). Again, there was no significant difference in the concentrations of MDA, 8-OHDG, and 8-iso-PGF2α between the M-MSN@NAC and the H/R groups, consistent with the results of ROS generation (all $p>0.05$) (Figure 6C–E).

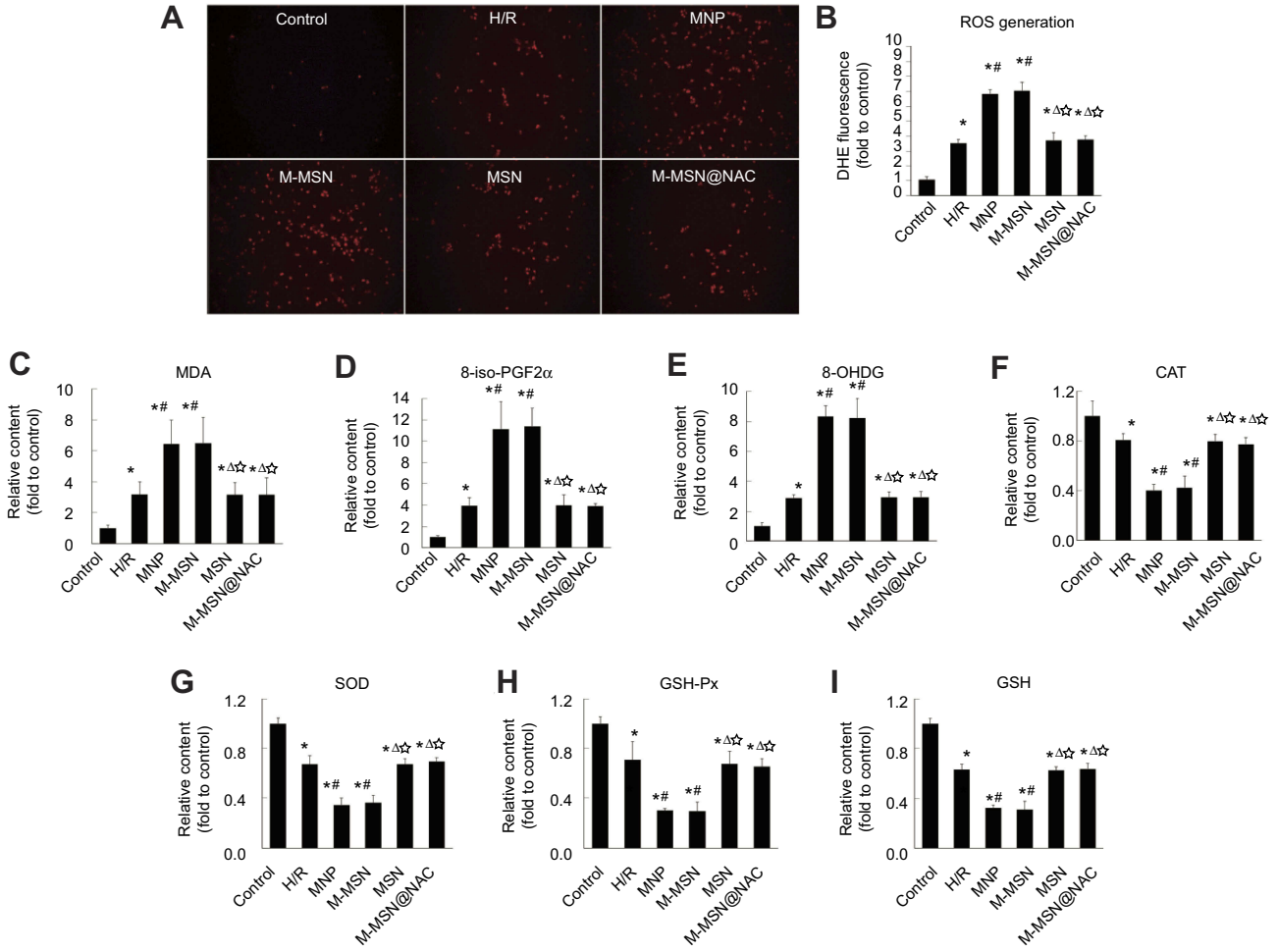

Figure 6 Effects of NPs exposure on ROS production and oxidant/antioxidant capacity. (**A**) Representative photomicrographs of intracellular ROS in cardiomyocytes visualized by fluorescent microscopy. Red fluorescent intensity indicated ROS accumulation. (**B**) Quantitative analysis of red fluorescent intensity in individual group. Data were collected from three independent experiments. (*p<0.001 vs Control; #p<0.001 vs H/R; Δp<0.01 vs MNP; ☆p<0.01 vs M-MSN). (**C-I**) Peroxide and antioxidant markers were measured by ELISA and biochemical analysis. Data were collected from three independent experiments. (*p<0.05 vs Control; #p<0.01 vs H/R; Δp<0.01 vs MNP; ☆p<0.01 vs M-MSN).

Abbreviations: NPs, nanoparticles; DHE, dihydroethidium; ROS,reactive oxygen species; MDA, malonaldehyde; 8-iso-PGF2α, 8-iso-prostaglandin F2α; 8-OHDG, 8-hydroxydeoxyguanine; GSH, glutathione; CAT, catalase; GSH-Px, glutathione peroxidase; SOD, superoxide dismutase; H/R, hypoxia/reoxygenation; MNP, magnetic iron oxide nanoparticles; MSN, mesoporous silica nanoparticles; M-MSN, magnetic mesoporous silica nanoparticles; M-MSN@NAC, M-MSN loaded with NAC.

Both the MNP group and the M-MSN group demonstrated dramatically lower levels of GSH, CAT, GSH-Px, and SOD than those in the H/R group by the biochemical assay (all p<0.01) (Figure 6F–I). Similarly, comparable results were found between the M-MSN@NAC and the H/R groups (all p>0.05) (Figure 6F–I).

Not surprisingly, ROS level of the control group was significantly lower than those of the four treatment groups and H/R group (all p<0.001) (Figure 6A and B). Accordingly, the control group demonstrated lower markers of oxidative stress and stronger antioxidant capacity than those of in the four treatment groups and H/R group (all p<0.05) (Figure 6C–I).

Taken together, these results suggest that MNPs and M-MSNs exacerbated peroxidation to lipids, proteins, and nucleic acids by inducing oxidative stress, leading to depletion of antioxidants and cellular damage in in vitro H/R cardiomyocytes. The imbalance is characterized by a significant increase of MDA, 8-iso-PGF2 alpha, and 8-OHDG levels and a steep reduction of GSH, CAT, GSH-Px, and SOD levels. Surprisingly, the M-MSN@NAC could alleviate oxidative stress damage induced by iron oxide NPs.

M-MSN@NAC alleviate overactivated ER stress and autophagy induced by MNPs or M-MSNs

To examine if MNPs and M-MSNs could induce ER stress response of H/R cardiomyocytes, the protein expression of

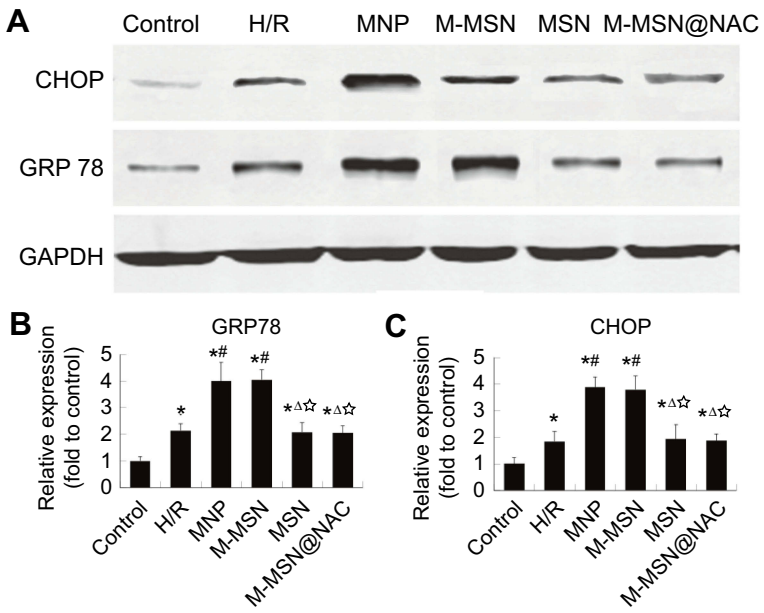

Figure 7 Effects of NPs exposure on activation of ER stress. (**A**) The expression of ER stress-associated proteins was detected by WB. (**B-C**) Quantitative analysis of CHOP and GRP78 using data from three independent experiments. (*p<0.01 vs Control; #p<0.0001 vs H/R; Δp<0.0001 vs MNP; ☆p<0.0001 vs M-MSN).
Abbreviations: NPs, nanoparticles; ER,endoplasmic reticulum; WB,Western Blotting; CHOP,CCAAT/enhancer binding protein-homologous protein; GRP78, glucose-regulated protein78; H/R, hypoxia/reoxygenation; MNP, magnetic iron oxide nanoparticles; MSN, mesoporous silica nanoparticles; M-MSN, magnetic mesoporous silica nanoparticles; M-MSN@NAC, M-MSN loaded with NAC.

two key markers of ER stress, CHOP and GRP78 were assessed by WB after exposure. Compared with the H/R group, both the MNP and M-MSN groups exhibited markedly elevated protein expression in CHOP and GRP78 (all p<0.0001) (Figure 7A–C). Notably, the markers of ER stress had no significant difference between the M-MSN@NAC group and the H/R group (p>0.05) (Figure 7A–C). Compared to the control group, the four treatment groups and H/R group showed significant increased expression of marker proteins of ER stress (all p<0.01) (Figure 7A–C).

To investigate whether MNPs and M-MSNs could activate autophagy of H/R cardiomyocytes, we examined LC3-I/II and p62 protein after exposure. Both the MNP group and M-MSN group exhibited that a higher expression of p62 and a more conversion from LC3-I to LC3-II than those in the H/R group by WB detection (all p<0.0001) (Figure 8A–C). Surprisingly too, the expressions of LC3-II and p62 protein were indistinguishable between the M-MSN@NAC and the H/R groups (p>0.05) (Figure 8A–C). This clearly suggests that ER stress and autophagy are resulted from ROS production caused by MNPs or M-MSNs exposure. The data suggest that the excessively activated ER stress and autophagy might be a downstream molecular mechanism of oxidative stress injury mediated by iron oxide NPs. Compared to the control group, the four treatment groups and H/R group showed significant increased expression of marker proteins of autophagy (all p<0.01) (Figure 8A–C).

Discussion

Oxidative stress is regarded as the major mechanism of iron oxide NPs-induced cell injury. Here, we developed an antioxidant magnetic iron oxide NPs named M-MSN@NAC, which effectively alleviated oxidative stress damage triggered by iron oxide through releasing active NAC to suppress the formation of oxidized cellular products.

The degradation of iron oxide NPs is a key determinant of their cytotoxicity.[24,25] When internalized into cells, the iron oxide NPs will be degraded in lysosomes and endosomes to release free iron ions (Fe^{2+}, Fe^{3+}). Then, the iron ions are available for Haber–Weiss–Fenton reactions to produce a large amount of ROS, resulting in oxidative stress injury.[24] It is well known that phagocytic capacity of cardiac myocytes is limited. Furthermore, unlike in vivo conditions, in vitro iron oxide NPs have no chance to be engulfed and degraded by mononuclear macrophages. Then, how can iron oxide NPs exert toxic effects on H/R cardiomyocytes in vitro?

Our data showed that H/R cardiomyocytes exhibited a higher ROS level relative to normal cardiomyocytes, suggesting that H/R per se can induce oxidative stress to

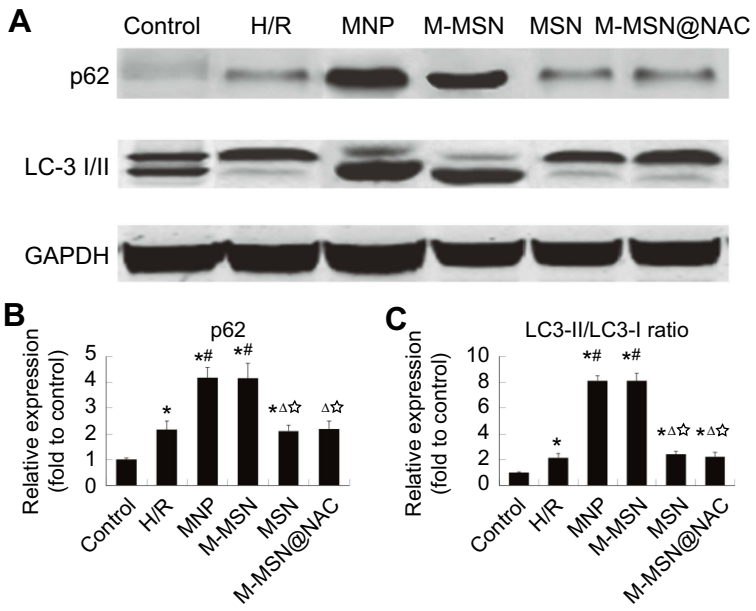

Figure 8 Effects of NPs exposure on autophagy induction. (**A**) The expression of autophagy-associated proteins was detected by WB. (**B-C**) Quantitative analysis of p62 and LC3-II/LC3-I ratio using data from three independent experiments. (*p<0.01 vs Control; #p<0.0001 vs H/R; Δp<0.0001 vs MNP; ☆p<0.0001 vs M-MSN).
Abbreviations: NPs, nanoparticles; WB,Western blotting; LC3-II/I, microtubule-associated protein light chain 3 II/I; H/R, hypoxia/reoxygenation; MNP, magnetic iron oxide nanoparticles; MSN, mesoporous silica nanoparticles; M-MSN, magnetic mesoporous silica nanoparticles; M-MSN@NAC, M-MSN loaded with NAC.

produce ROS, including H_2O_2, superoxide, hydroxyl radical, and singlet oxygen,[26] which exceeded the capacity of anti-oxidant of cardiomyocytes, leading to oxidative damage. Fe_3O_4 NPs and H_2O_2 have been proved to be an efficient heterogeneous Fenton reaction system at a wider pH range (2–9) for environmental applications.[27,28] Therefore, there is a possibility that H_2O_2 leaking from injured cardiomyocytes reacts with Fe_3O_4 NPs by heterogeneous Fenton reaction, generating a large number of toxic hydroxyl radicals which resulted in accelerated oxidative damage. In addition, a small amount of iron oxide engulfed by myocardial cells could be degraded into Fe^{2+} and Fe^{3+} ions in the lysosomes, and the free iron ions could catalyze the conversion of H_2O_2 into hydroxyl radicals by homogeneous Fenton reaction. We speculated that heterogeneous Fenton reaction may be the main mechanism of iron oxide-induced cell injury in our work.

Theoretically, the amino and carboxyl groups of NAC could form hydrogen bonds with a large amount of Si-OH on the inner and outer surfaces of M-MSNs. However, NAC and water formed stronger hydrogen bonds in the aqueous phase, leading to hardly load NAC into the M-MSNs. To overcome this limitation, chloroform was chosen to minimize the competitive interactions between the solvent and either NAC or M-MSNs. The loading amount of NAC with M-MSNs was 200 μg/mg by the UV-vis method as described previously,[20] indicating that NAC was successfully loaded into the M-MSNs in the initial solution, which should ascribe to the non-polar solvent strategy. The constant proportion of Fe_3O_4, NAC, and MSN of M-MSN@NAC is 6%, 13.8%, and 80.2%, respectively.

In a previous study, rat iron overload was established by intraperitoneal injection of iron-dextran (300 mg/kg once), leading to oxidative damage of heart and liver. This oxidative damage was partly attenuated by subcutaneous injection of NAC (150 mg/kg once), in which the ratio of iron dextran to NAC content was 2:1.[29] Considering the constant proportion of Fe_3O_4/NAC in the M-MSN@NAC is 1:2.3, we established a single dose of 50 μg Fe_3O_4 for the corresponding dose of M-MSN@NAC (the total amount of 718.34 μg, including Fe_3O_4 50 μg, MSN 668.34 μg, and NAC 115 μg). The proportion of NAC in M-MSN@NAC is significantly higher than that in the previous study, ensuring the effective concentrations of NAC released into the target site. Moreover, unlike separate or sequential antioxidant administration,[29–31] M-MSN@NAC enable both iron oxide NPs and antioxidants to simultaneously act on the same target site, facilitating local high concentrations of NAC to play a beneficial anti-oxidant role. Our results demonstrated that M-MSN@NAC could minimize the toxic effects of iron oxide on H/R cardiomyocytes in a 24-hr exposure, indicating that M-MSN@NAC have a better biocompatibility than MNPs or M-MSNs.

In the present study, the anti-oxidative M-MSN@NAC not only alleviated MNPs or M-MSNs-induced injury of H/R cardiomyocytes but significantly inhibited ER stress and hyperactivation of autophagy by reducing the expression of GRP78, CHOP, p62, and the conversion from LC3-I to LC3-II. These results indicate that hyperactivation of ER stress and autophagy may be a downstream pathological mechanism of oxidative stress injury induced by acute iron oxide exposure. Previous studies suggested that multiple mechanisms were involved in Fe_3O_4 NPs-induced autophagosome accumulation, in which autophagy was attributed to the damage of lysosomes, mitochondrial, ER, and Golgi body.[14,32] Necrosis type cell death was caused by iron oxide NPs-induced ROS and autophagy, and the classical mTOR pathway was found to promote cell death in lung cancer cells (A549).[15] The autophagy preceding apoptosis was induced as a result of mitochondrial dysfunction and ER stress caused by MNPs in RAW264.7 cells.[14] Thus, the molecular mechanisms of toxic effects of iron oxide NPs may be involved in more complicated cell signaling pathways and molecular networks which are needed to be further investigated.

Our data revealed that there was no difference in detection of oxidative stress, ER stress, autophagy as well as cell apoptosis between the MNP and M-MSN groups, suggesting that Fe_3O_4 NPs with or without MSNs coating had no significant difference in toxic effects on H/R cardiomyocytes. Similarly, both the MSN group and the H/R group had no significant difference in oxidative stress, ER stress, autophagy as well as cell apoptosis, indicating that MSNs did not significantly induce extra oxidative stress of H/R cardiomyocytes as a result of good biocompatibility, consistent with the previous study.[33] Therefore, MSNs can be used as an ideal drug carrying structure for NAC loaded on MNPs.

Our study first showed that M-MSN@NAC could effectively suppress iron oxide-induced H/R cardiomyocytes damage in a short term, suggesting that the strategy of MNPs loaded with antioxidants bears a potential to improve the biocompatibility of MNPs with target organs. When antioxidant-modified MNPs are used as therapeutic substance carriers (including drug, gene or cell) or magnetic resonance contrast agents in clinical setting, the safety of MNPs is expected to be significantly improved.

Study limitations

First, the toxicity of different coatings or different types of iron oxide NPs may be different and need to be investigated in detail. Second, we observed a trend that MNPs or M-MSNs could increase apoptosis of H/R cardiomyocytes after 24 hrs exposure, but failed to reach statistical significance. Considering that previous study has confirmed cytotoxicity of iron oxide is concentration- and time-dependent,[3,10] our findings may be related to short observation (24 hrs) and relative low concentration of iron oxide NPs (Fe_3O_4 50 μg). A longer-exposure time and higher-concentration observation are needed to further clarify the cytotoxicity of MNPs or M-MSNs and antioxidant effects of NAC. Third, when applied to the ischemia myocardium, long-term retention of iron oxide NPs in ischemia myocardium could cause chronic iron overload, leading to more severe oxidative stress injury by exacerbating inflammation after myocardial infarction,[8] and degrading more iron oxide through recruited macrophages. Thus, it is necessary to further investigate the chronic toxic effects and the underlying mechanisms and to verify whether M-MSN@NAC can also play a long-term protective role in vivo.

Conclusions

M-MSN@NAC can significantly mitigate iron oxide NPs-induced oxidative stress of H/R cardiomyocytes by releasing NAC to reduce the generation of peroxidation products. Antioxidant loaded on iron oxide NPs provides novel insight into the strategy to improve the biocompatibility of MNPs with target organs.

Acknowledgments

The authors gratefully acknowledge the financial support from the National Natural Science Foundation of China (grant/award numbers: 81500201, 81570223, 81500191, and 81870296) and the Key Disciplines Group Construction Project of Pudong Health Bureau of Shanghai (grant/award number: PWZxq2017-05).

Disclosure

The authors report no conflicts of interest in this work.

References

1. Mohanty S, Jain KG, Nandy SB, et al. Iron oxide labeling does not affect differentiation potential of human bone marrow mesenchymal stem cells exhibited by their differentiation into cardiac and neuronal cells. *Mol Cell Biochem*. 2018;448(1–2):17–26. doi:10.1007/s11010-018-3309-9
2. Shen Y, Huang Z, Liu X, et al. Iron-induced myocardial injury: an alarming side effect of superparamagnetic iron oxide nanoparticles. *J Cell Mol Med*. 2015;19(8):2032–2035. doi:10.1111/jcmm.12582
3. Gaharwar US, Meena R, Rajamani P. Iron oxide nanoparticles induced cytotoxicity, oxidative stress and DNA damage in lymphocytes. *J Appl Toxicol*. 2017;37(10):1232–1244. doi:10.1002/jat.3485

4. Murphy CJ, Oudit GY. Iron-overload cardiomyopathy: pathophysiology, diagnosis, and treatment. *J Card Fail*. 2010;16(11):888–900. doi:10.1016/j.cardfail.2010.05.009
5. Gordan R, Wongjaikam S, Gwathmey JK, et al. Involvement of cytosolic and mitochondrial iron in iron overload cardiomyopathy: an update. *Heart Fail Rev*. 2018;23(5):801–816. doi:10.1007/s10741-018-9700-5
6. Nemmar A, Beegam S, Yuvaraju P, et al. Ultrasmall superparamagnetic iron oxide nanoparticles acutely promote thrombosis and cardiac oxidative stress and DNA damage in mice. *Part Fibre Toxicol*. 2016;13(1):22. doi:10.1186/s12989-016-0132-x
7. Manickam V, Periyasamy M, Dhakshinamoorthy V, et al. Recurrent exposure to ferric oxide nanoparticles alters myocardial oxidative stress, apoptosis and necrotic markers in male mice. *Chem Biol Interact*. 2017;278:54–64. doi:10.1016/j.cbi.2017.10.003
8. Huang Z, Li C, Yang S, et al. Magnetic resonance hypointensive signal primarily originates from extracellular iron particles in the long-term tracking of mesenchymal stem cells transplanted in the infarcted myocardium. *Int J Nanomedicine*. 2015;10:1679–1690. doi:10.2147/IJN.S77858
9. Wu X, Tan Y, Mao H, et al. Toxic effects of iron oxide nanoparticles on human umbilical vein endothelial cells. *Int J Nanomedicine*. 2010;5:385–399.
10. Naqvi S, Samim M, Abdin M, et al. Concentration-dependent toxicity of iron oxide nanoparticles mediated by increased oxidative stress. *Int J Nanomedicine*. 2010;5:983–989. doi:10.2147/IJN.S13244
11. Srinivas A, Rao PJ, Selvam G, et al. Oxidative stress and inflammatory responses of rat following acute inhalation exposure to iron oxide nanoparticles. *Hum Exp Toxicol*. 2012;31(11):1113–1131. doi:10.1177/0960327112446515
12. Wang C, Jia H, Zhu L, et al. Toxicity of alpha-Fe2O3 nanoparticles to Artemia salina cysts and three stages of larvae. *Sci Total Environ*. 2017;598:847–855. doi:10.1016/j.scitotenv.2017.04.183
13. Hanini A, Schmitt A, Kacem K, et al. Evaluation of iron oxide nanoparticle biocompatibility. *Int J Nanomedicine*. 2011;6:787–794. doi:10.2147/IJN.S17574
14. Park EJ, Choi DH, Kim Y, et al. Magnetic iron oxide nanoparticles induce autophagy preceding apoptosis through mitochondrial damage and ER stress in RAW264.7 cells. *Toxicol In Vitro*. 2014;28(8):1402–1412. doi:10.1016/j.tiv.2014.07.010
15. Khan MI, Mohammad A, Patil G, et al. Induction of ROS, mitochondrial damage and autophagy in lung epithelial cancer cells by iron oxide nanoparticles. *Biomaterials*. 2012;33(5):1477–1488. doi:10.1016/j.biomaterials.2011.10.080
16. Wongjaikam S, Kumfu S, Khamseekaew J, et al. Combined iron chelator and antioxidant exerted greater efficacy on cardioprotection than monotherapy in iron-overloaded rats. *PLoS One*. 2016;11(7):e0159414. doi:10.1371/journal.pone.0159414
17. Kumfu S, Khamseekaew J, Palee S, et al. A combination of an iron chelator with an antioxidant exerts greater efficacy on cardioprotection than monotherapy in iron-overload thalassemic mice. *Free Radic Res*. 2018;52(1):70–79. doi:10.1080/10715762.2017.1414208
18. Zhang J, Li X, Rosenholm JM, et al. Synthesis and characterization of pore size-tunable magnetic mesoporous silica nanoparticles. *J Colloid Interface Sci*. 2011;361(1):16–24. doi:10.1016/j.jcis.2011.05.038
19. Xu H, Cui L, Tong N, et al. Development of high magnetization Fe3O4/polystyrene/silica nanospheres via combined miniemulsion/emulsion polymerization. *J Am Chem Soc*. 2006;128(49):15582–15583. doi:10.1021/ja066165a
20. Eid MA. Spectrophotometric determination of cysteine and N-Acetylcysteine in pharmaceutical preparations. *Mikrochim Acta*. 1998;129:5.
21. Wu WY, Li YD, Cui YK, et al. The natural flavone acacetin confers cardiomyocyte protection against hypoxia/reoxygenation injury via AMPK-mediated activation of Nrf2 signaling pathway. *Front Pharmacol*. 2018;9:497. doi:10.3389/fphar.2018.00497
22. Chen J, Rogers SC, Kavdia M. Analysis of kinetics of dihydroethidium fluorescence with superoxide using xanthine oxidase and hypoxanthine assay. *Ann Biomed Eng*. 2013;41(2):327–337.
23. Towbin H, Staehelin T, Gordon J. Electrophoretic transfer of proteins from polyacrylamide gels to nitrocellulose sheets: procedure and some applications. *Proc Natl Acad Sci U S A*. 1979;76(9):4350–4354. doi:10.1073/pnas.76.9.4350
24. Singh N, Jenkins GJ, Nelson BC, et al. The role of iron redox state in the genotoxicity of ultrafine superparamagnetic iron oxide nanoparticles. *Biomaterials*. 2012;33(1):163–170. doi:10.1016/j.biomaterials.2011.09.087
25. Luo C, Li Y, Yang L, et al. Superparamagnetic iron oxide nanoparticles exacerbate the risks of reactive oxygen species-mediated external stresses. *Arch Toxicol*. 2015;89(3):357–369. doi:10.1007/s00204-014-1267-x
26. Hayyan M, Hashim MA, AlNashef IM. Superoxide ion: generation and chemical implications. *Chem Rev*. 2016;116(5):3029–3085. doi:10.1021/acs.chemrev.5b00407
27. Hua Z, Ma W, Bai X, et al. Heterogeneous Fenton degradation of bisphenol A catalyzed by efficient adsorptive Fe3O4/GO nanocomposites. *Environ Sci Pollut Res Int*. 2014;21(12):7737–7745. doi:10.1007/s11356-014-2728-8
28. Wang W, Mao Q, He H, et al. Fe3O4 nanoparticles as an efficient heterogeneous Fenton catalyst for phenol removal at relatively wide pH values. *Water Sci Technol*. 2013;68(11):2367–2373. doi:10.2166/wst.2013.497
29. Lou LX, Geng B, Chen Y, et al. Endoplasmic reticulum stress involved in heart and liver injury in iron-loaded rats. *Clin Exp Pharmacol Physiol*. 2009;36(7):612–618. doi:10.1111/j.1440-1681.2008.05114.x
30. Sadeghi L, Tanwir F, Yousefi Babadi V. Antioxidant effects of alfalfa can improve iron oxide nanoparticle damage: invivo and invitro studies. *Regul Toxicol Pharmacol*. 2016;81:39–46. doi:10.1016/j.yrtph.2016.07.010
31. Cochran DB, Wattamwar PP, Wydra R, et al. Suppressing iron oxide nanoparticle toxicity by vascular targeted antioxidant polymer nanoparticles. *Biomaterials*. 2013;34(37):9615–9622. doi:10.1016/j.biomaterials.2013.08.025
32. Zhang X, Zhang H, Liang X, et al. Iron oxide nanoparticles induce autophagosome accumulation through multiple mechanisms: lysosome impairment, mitochondrial damage, and ER stress. *Mol Pharm*. 2016;13(7):2578–2587. doi:10.1021/acs.molpharmaceut.6b00405
33. Sadeghnia HR, Zoljalali N, Hanafi-Bojd MY, et al. Effect of mesoporous silica nanoparticles on cell viability and markers of oxidative stress. *Toxicol Mech Methods*. 2015;25(6):433–439.